THE GLAS PHYSICAL NUMERICAL ALGORITHM FOR ANALYSIS OF HIRS 2/MSU DATA

J. Susskind
NASA/GLAS
Greenbelt, MD
USA

and

M.T. Chahine
Jet Propulsion Laboratory
Pasadena, CA
USA

1. Introduction

The GLAS physical inversion algorithm for analysis of HIRS-2/MSU data is basically the same as that reported in Susskind and Rosenfield (1980) and expanded on in Susskind et al. (1982). The current method is an evolutionary outgrowth of earlier research and experience that began with analysis of VTPR data on NOAA-2 and NOAA-4 (Jastrow and Halem, 1973; Halem and Susskind, 1977) and continued with work on HIRS/SCAMS data from NIMBUS 6 (Halem et al., 1978). The analysis procedures are based primarily on the relaxation scheme and cloud filtering methods given in Chahine (1970, 1974).

The principle of the physical inversion algorithm is to find atmospheric and surface conditions, which, when substituted in the multi-spectral radiative transfer equations representing the dependence of the observations in the various channels on geophysical parameters, match those observations to a specified level. If no such solution can be found, the retrieval is rejected. Hence, one of the critical elements of the system is the ability to compute the forward problem, that is, the radiances the instrument would see as a function of atmospheric and surface conditions. The details of the radiative transfer calculations used at GLAS and the form of a rapid algorithm used to model transmittances as a function of temperature-humidity-ozone profile and zenith angle are described in Susskind et al., (1982, 1983). It is shown that after minor empirical corrections to the transmittance functions, which are transferable from one season to another, observed brightness temperature agree with those computed from colocated oceanic radiosondes to an RMS difference of about .7°C under clear conditions. Under partially cloudy conditions, RMS differences of computed radiances with reconstructed clear column radiances degrade to the order of 1°C. Using our retrieval algorithm, it is shown that these errors contribute about 80% of their value to errors in retrieved temperature profiles. No specific corrections have to be made for zenith angle and surface elevation other than to substitute the appropriate quantities in the radiative transfer equations. The surface temperature and emissivity at 50.3 GH_z are determined as part of the iterative scheme. The emissivity in the infra-red regions is set at prescribed values for land and water.

The basic elements of the retrieval scheme are:

- Grouping spots into fields of view,
- Attaching initial guess conditions,
- Computing radiances from the initial guess,
- Determining the emissivity at 50.3 GH,
- Estimating N^{th} clear column radiances,
- Retrieving N^{th} ground temperature,
- Retrieving N^{th} atmospheric temperature profile,

- Computing N^{th} guess radiances which are compared with N^{th} clear column radiances for convergence. If sufficient agreement is not reached, return to emissivity determination.

Here we will briefly outline some of the important elements of the scheme.

2. Grouping of Spots

Retrievals are done using a "two field of view" approach (Smith, 1968; Chahine 1974) to correct (reconstruct) observed radiances to what they would have been if no clouds were present. The two fields of view should represent similar meteorological conditions but with one field of view having greater cloud amount that the other. Two types of retrievals have been done, global and regional scale. In the global retrievals, one retrieval is done every 250 x 250 km. This area is subdivided into four 125 x 125 km sub-areas, each containing a number of HIRS2 spots (decreasing with increasing zenith angle). These spots are sub-divided into the half (field of view 1) with the warmest 11μm window observations and the half with the coldest (field of view 2). Radiances for all spots in each field of view are averaged together for each channel, giving radiances for 2 fields of view for each channel in each sub-area. The MSU observation closest to the center of the sub-area containing the warmest 11μm observation in the warm field of view (field of view 1) is chosen as the sub-area for which a retrieval is done. In the case of regional retrievals, an analogous procedure is used, but this time the areas for retrieval are always taken as 4 x 4 groups of HIRS-2 spots and the sub-areas as 2 x 2 groups. Currently, global retrievals have been run for January, February, May, June, July, and November 1979 from TIROS-N data. Regional retrievals have been run for only three cases thus far, one of which will be shown this report. We are currently in the process of computing transmittance functions and empirical corrections for NOAA-7 HIRS channels and were not ready to analyze the selected NOAA-7 cases at this time.

3. Clear Column Radiance Algorithm

Given radiances for channel i in two fields of view, $R_{i,1}$ and $R_{i,2}$, clear column radiances, $\hat{R}_i$, are reconstructed according to

$$\hat{R}_i = R_{i,1} + n(R_{i,1} - R_{i,2}) \tag{1}$$

Once n is obtained in a given iteration, $\hat{R}_i$ is used to determine ground and atmospheric temperatures. We determine n from combined observations in HIRS-2 channel 13 (2190 cm^{-1}) and MSU channel 2 (53.7 GH_z) according to

$$n^N = \frac{B_{13}(T_{B,13} + T_2 - T_2^N) - R_{13,1}}{R_{13,1} - R_{13,2}} \tag{2}$$

where $R_{13,i}$ is the radiance for channel 13 in field of view i, $T^N_{B,13}$ is the brightness temperature for channel 13 computed using the N^{th} guess temperature profile and ground temperature, T_2 and T_2^N are the observed and computed brightness temperatures for MSU channel 2, and $B_{13}[T]$ is the black-body function evaluated at the central frequency of channel 13. The term in brackets represents the microwave corrected estimated clear column brightness temperature for channel 13. The addition of $T_2 - T_2^N$ to $T^N_{B,13}$ corrects, to first order, for errors and $T^N_{B,13}$ due to errors in the initial (or N^{th}) guess temperature profile.

Special cases occur for clear (n=-.5) and full overcast (n=∞) conditions. If the denominator of equation (2) is small, assessment of the numerator in equation (2) is used to distinguish between these extremes. The latter case, indicated by large n, is rejected as too cloudy to do a retrieval. This happens globally about 8% of the time. In addition, if the numerator is negative, n is taken as zero, that is, field of view 1 is assumed to be clear. More details are given in Susskind et al., (1982).

4. Ground Temperature

Given the reconstructed clear column radiances for all channels, ground temperature at night can be solved for in a straightforward manner from any of the three window channels 8, 18, and 19, according to

$$T_{s,i} = B_i^{-1} \left[\frac{\hat{R}_i - R_{ATM}}{\varepsilon_i \, \tau_i(P_s)} \right] \tag{3}$$

where $\hat{R}_i$ is the clear column radiance, R_{ATM} is the upwelling radiation emitted by the atmosphere, including that component reflected off the surface, ε_i is the surface emissivity, and $\tau_i(P_s)$ is the atmospheric transmittance for channel i. The transmittance depends primarily on the water vapor distribution, which in our analysis thus far, is constrained to be that of the first guess field (we are just beginning work on humidity retrievals). The transmittances in channels 18 and 19 (4.0 and 3.7 μm) are much less sensitive to humidity than those in channel 8 (11μm). In addition to the uncertainty in transmittance due to errors in the estimated humidity profile, channel 8 is less suitable for use as a window channel because under very humid conditions, $\tau_8(p_s)$ can become as low as .2. Therefore, we use channels 18 and 19 to obtain ground temperature and set $T_s = 1/2 \, (T_{s,18} + T_{s,19})$. The emissivity in equation 3 is assumed to be .85 over land and .95 over ocean for channels 18 and 19.

During the day, one has to consider the effects on channels 18 and 19 of solar radiation reflected off the ground. Solar radiation reflected off clouds is assumed to be accounted for by the clear-column radiance algorithm. One can write

$$(\hat{R}_i - R_{ATM})/\varepsilon_i\tau_i = B_i(T_s) + \rho_i H_i \tau_i'/\tau_i = A_i \quad (4)$$

where ρ_i is the unknown bi-directional reflectance in channel i of solar radiation reflected off the ground in the direction of the satellite, H_i is the known incoming solar radiation, and τ_i' is the calculated atmospheric transmittance along the entire path from the sun to the ground to the satellite. The left hand side is known, as in equation (3). If we assume $\rho_{18}=\rho_{19}$, then T_s can be solved for by the non-linear equation

$$B_{18}(T_s) - \alpha B_{19}(T_s) = A_{18} - \alpha A_{19} \quad (5)$$

where α is given by H_{18}'/H_{19}' and $H'= H_i\tau_i'/\tau_i$.

We currently use this procedure during the day in all cases. We are investigating the use of channel 8 to determine ground temperatures during the day under conditions where the solar correction to the brightness temperatures in channels 18 and 19 appears large while the effect of humidity on channel 8 appears small.

5. Atmospheric Temperature Profile Relaxation Equation

Given reconstructed clear column radiances $\hat{R}_i^N$, we determine the reconstructed clear column brightness temperatures, $\hat{T}_{B,i}^N$, and compare them to $T_{B,i}^N$, the computed brightness temperatures from the N^{th} guess temperature profile and ground temperature. The differences $[\hat{T}_{B,i}^N - T_{B,i}^N]$ are used in the temperature sounding channels to update the atmospheric temperature profile. We use the relaxation equation

$$\overline{T}_j^{N+1} = \overline{T}_j^N + \Sigma_i \overline{W}_{ij}[\hat{T}_{B,i}^N - T_{B,i}^N]/\Sigma_i \overline{W}_{ij} \quad (6)$$

where $\overline{T}_j$ is the layer mean temperature in atmospheric layer j, and $\overline{W}_{ij}$ is the layer average temperature sensitivity function for channel i in layer j where $W_i(P)$ is given by Susskind and Rosenfield, 1980

$$W_i(P) = \left[\frac{dT_{Bi}}{dR_i}\right]_{R_i} \left[\frac{dR_i}{dT}\right]_{T(P)} \quad (7)$$

$$= \left[\frac{dB_i}{dT}\right]^{-1}_{T_{B,i}} \left[\frac{dB_i}{dT}\right]_{T(P)} \left[\frac{d\tau_i}{d\ln P}\right]_P$$

Figure 1 shows the sensitivity functions for the seven channels we use to update the temperature profile and the 10 atmospheric layers used in equation (6). The 10 layer mean temperatures do not uniquely define a temperature profile. We constrain all our solutions to be of the form

$$T^N(P) = T^G(P) + \sum_{k=1}^{L} A_k^N F_k(P) \qquad (8)$$

where $T^G(P)$ is a global mean temperature profile and $F_k(P)$ are the L eigenfunctions of a covariance matrix of atmospheric temperature profiles which explain the most atmospheric variance. Given estimates of the vector $\overline{T}^N$, the vector A^N is determined according to

$$A^N = [\overline{F}'\overline{F} + \sigma H]^{-1} \overline{F}'[\overline{T} - \overline{T}_G] \qquad (9)$$

where $\overline{F}_j$ is the layer average of $F_k(P)$ in layer j and H is a diagonal matrix with H_{ii} being the inverse of the fraction of variance arising from eigenvector i and σ is a constant. We use L = 6 and $\sigma = 5\text{x}10^{-4}$ in equations (8) and (9).

Additional pieces of information can also be added to equation (9) to determine A^N provided the equations are linear functions of T(P). For example, if the temperature is known at a given level of the atmosphere, or the lapse rate is known, that is, the difference of temperatures is known at two levels of the atmosphere, additional rows can be added to $\overline{F}$, $\overline{T}$, and $\overline{T}_G$ where the bar represents the specific quantity such as value (or difference) of $F_k(P)$ and T(P) at the appropriate level (or levels). In our analysis thus far, we have found that the retrieved ground temperature closely matches colocated radiosonde surface air temperatures under conditions when the ground temperature is colder than the radiosonde 850 mb temperature, especially if large inversions exist. Therefore, we provide an additional piece of information to equation (9) defining the surface air temperature as the retrieved ground temperature over land if the ground temperature is colder than the estimated 850 mb temperature.

6. Sample Case

A case was selected randomly from SOP-1 (1/22/79 0225GMT) of FGGE to compare the operational retrievals with those we generated in the global and regional modes for the ALPEX area. Figure 2 shows the location and types of retrievals and the values of the 700 mb temperatures determined in each mode and also the radiosonde reports at 1/22/79 0000GMT. The temperatures are given in °C x 10 with the first digit understood (i.e. 699 means 269.9°C) For the GLAS retrievals, * mean n > 0, that is, neither field of view was considered clear. For the NESDIS operational retrievals, * means a cloud correction was made to the HIRS-2 observations while ** means microwave only retrievals were performed. The operational retrievals are for the most part treated as clear, with the exception of the southwestern corner of the scene, in which a number of microwave only retrievals were performed. The GLAS physical retrieval scheme produced partially cloudy retrievals over most of the southern portion of the scene, including the area in which microwave only retrievals were produced operationally. The GLAS regional scale retrievals are not only denser, as expected, but also produced more successful retrievals in the mountainous area in the vicinity of 50 N, 10 E. On the other hand, no

retrievals were accepted South-East of 20 E, 43 N. These retrievals were rejected primarily because of inconsistency of the IR observations with those of MSU channel 2, which covers a large spot of varied scene.

Figure 3 shows some of the other parameters obtained from the regional mode GLAS retrievals: ground temperature, surface emissivity at 50.3 GHz, and effective cloud fraction and cloud top temperature. Global monthly mean fields of these parameters have been produced for the six months of 1979 currently processed in the global mode. The ground temperatures (Figure 3a) are indicated using the same convention as the 700 mb temperatures in Figure 2. The emissivity (Figure 3b) at 50.3 GHz is indicated in percent. Land typically has values close to 1 while water surfaces are closer to .6. Mixed areas in the field of view contain intermediate values. This emissivity is used in computing the brightness temperatures for MSU channel 2. It is also an indicator of sea-ice ($\varepsilon > .7$) and snow cover over land ($\varepsilon < .9$). Neither of these appear in this scene, except for possibly in the vicinity of 8°E, 47°N. The cloud fractions (Figure 3c) are given in %. The cloud top pressures (Figure 3d) are given in millibars.

Figures 4-8 show thickness contours (in decameters) derived from the three sets of retrievals with the radiosonde reports indicated on the figures. The 700-1000 mb thickness fields and the 500-1000 mb thickness fields are quite similar to each other and are in general agreement with the radiosondes. The fields of the GLAS retrievals are generally closer to each other than they are to the operational field. Differences in patterns increase with increasing height in the 500-700 mb thickness, 300-500 mb thickness, and 100-300 mb thickness fields. The general agreement with radiosondes in the GLAS fields appears to be somewhat better, especially in the 100-300 mb thickness field, in which the operational retrievals appear to have a cold bias of about 60 meters and show a somewhat flatter field than indicated by the GLAS retrievals.

The specific NOAA-7 case studies selected by the workshop will be processed as soon as possible and will be sent to the workshop at a later date for inclusion in the workshop report if possible.

References

Chahine, M.T., 1970: Inverse problems in radiative transfer: determination of atmospheric parameters. J. Atmos. Sci., 27, 960-967.

Chahine, M.T., 1974: Remote sounding of cloudy atmospheres. I. The single cloud layer. J. Atmos. Sci., 31, 233-243.

Halem, M. and J. Susskind, 1977: The GISS VTPR processing manual. NASA Report X-130-77-53. Goddard Space Flight Center, Greenbelt, MD 20771.

Halem, M., M. Ghil, R. Atlas, J. Susskind, and W. Quirk, 1978: The GISS sounding temperature impact test. NASA Technical Memorandum 78063, pp. 2-9 to 2-82. Goddard Space Flight Center, Greenbelt, MD 20771.

Jastrow, R. and M. Halem, 1973: Accuracy and coverage of temperature data derived from the IR radiometer on the NOAA 2 satellite. J. Atmos. Sci., 30, 958-964.

Smith, W.L., 1968: An improved method for calculating tropospheric temperature and moisture from satellite radiometer measurements. Mon. Wea. Rev., 96, 387-396.

Susskind, J. and J. Rosenfield, 1980: The GLAS physical inversion method for analysis of TIROS-N data. VAS Demonstration Sounding Workshop, NASA Conference Publication 2147, pp. 41-55. NASA/Goddard Space Flight Center, July 15, 1980.

Susskind, J., J. Rosenfield, D. Reuter, and M.T. Chahine, 1982: The GLAS physical inversion method for analysis of HIRS2/MSU sounding data. NASA Tech. Memo. 84936.

Susskind, J., J. Rosenfield, and D. Reuter, 1983: An accurate radiative transfer model for use in the direct physical inversion of HIRS2 and MSU temperature sounding data. J. Geophys. Res., 88C, 8550-8568.

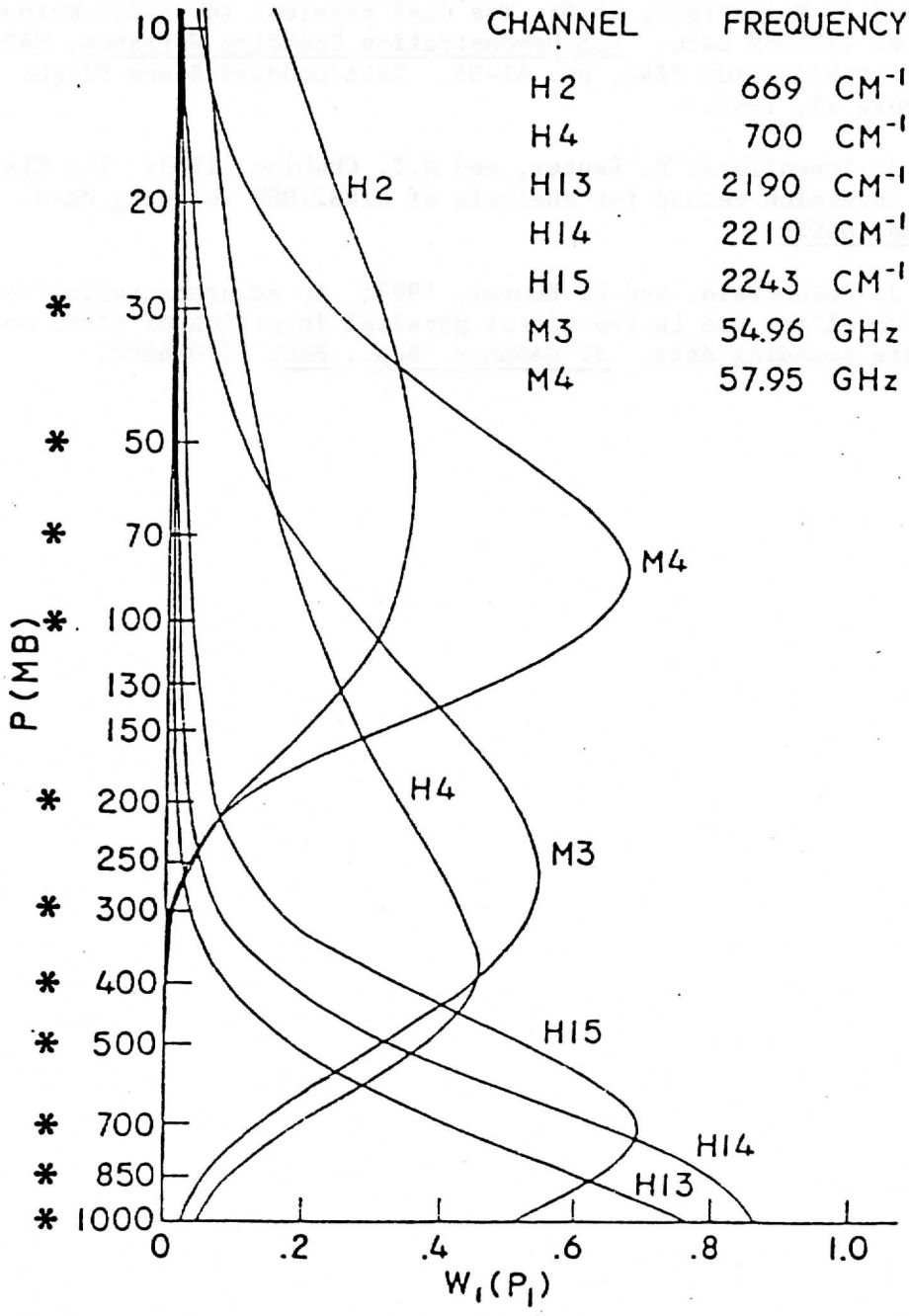

Figure 1. Temperature sensitivity functions for U.S. standard atmosphere at nadir viewing for the seven HIRS/MSU channels used to determine the temperature profile. These channels are used to estimate mean temperatures for the layers bounded by *.

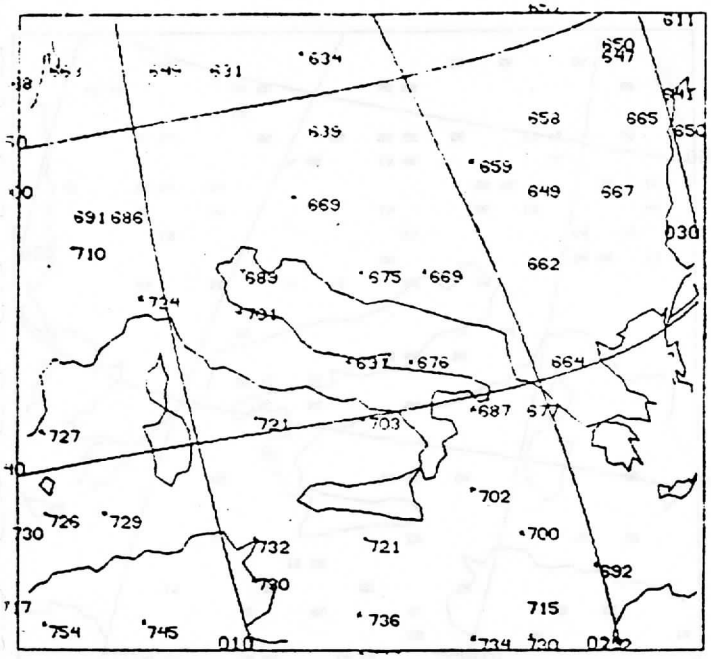

Figure 2a. Location of retrievals and 700 mb temperatures for the GLAS global retrievals. * indicates retrieval performed with cloud corrected radiances. Values in °C x 10 - 200. Soundings at 1/22 0230Z.

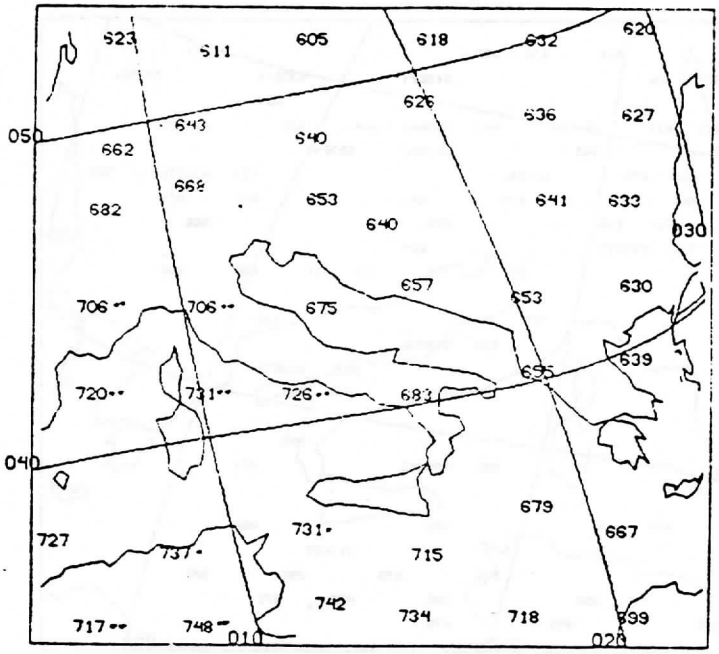

Figure 2b. Same as figure 2a for NESDIS operational retrievals. * indicates retrieval performed with cloud corrected radiances. ** indicates microwave only retrieval.

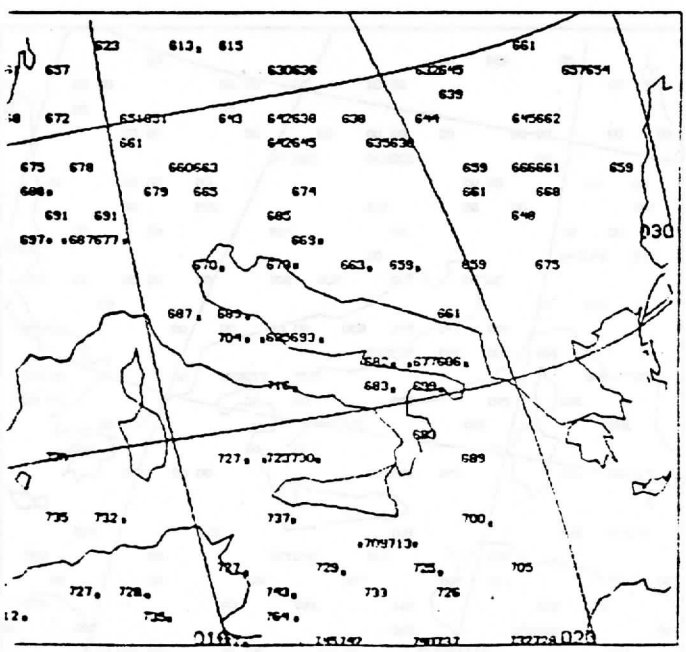

Figure 2c. Same as figure 2a but for GLAS regional retrievals.

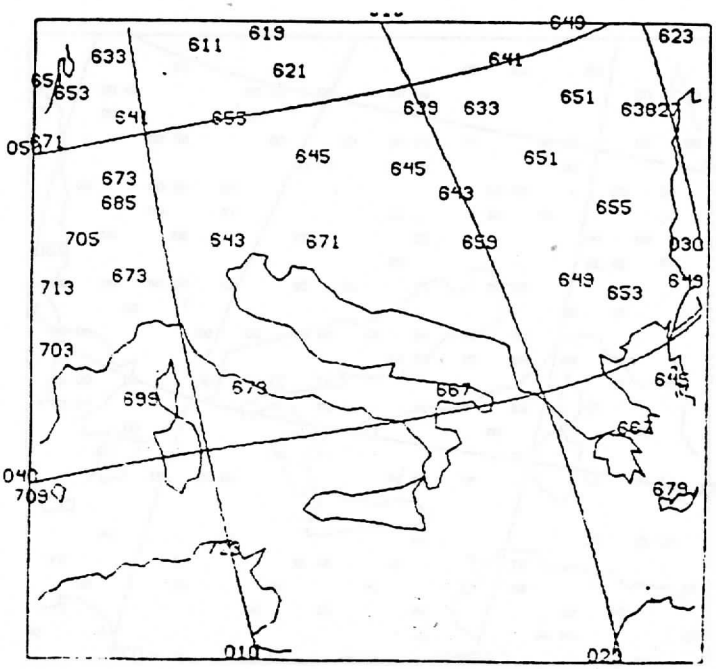

Figure 2d. Colocated radiosondes 700 mb temperature reports. 1/22 0000Z.

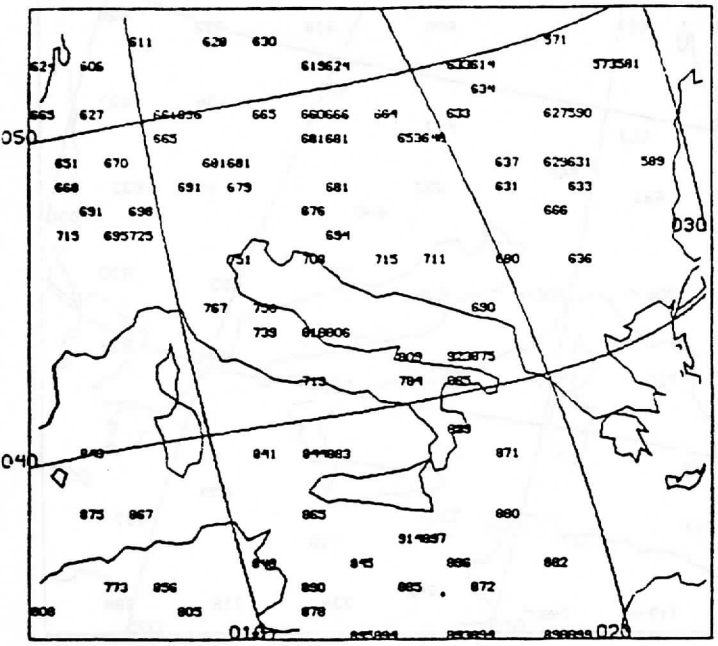

Figure 3a. Ground temperature obtained from GLAS regional scale retrievals (°C x 10-200).

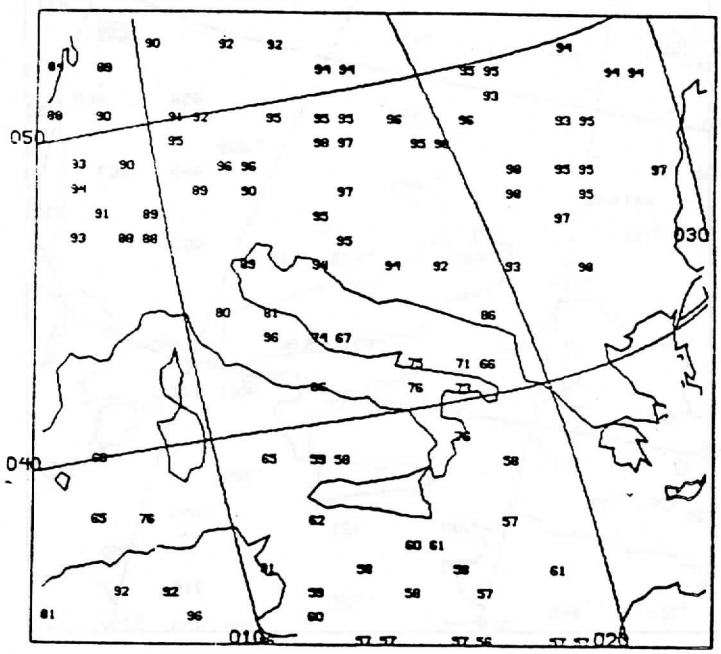

Figure 3b. Surface emissivity at 50.3 GHz (%) obtained from GLAS regional scale retrievals.

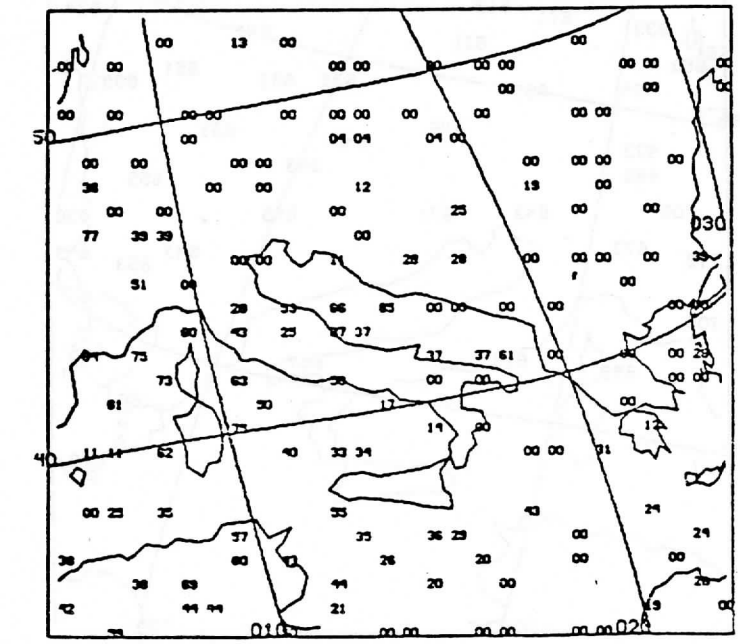

Figure 3c. Cloud fraction (%) obtained from GLAS regional scale retrievals.

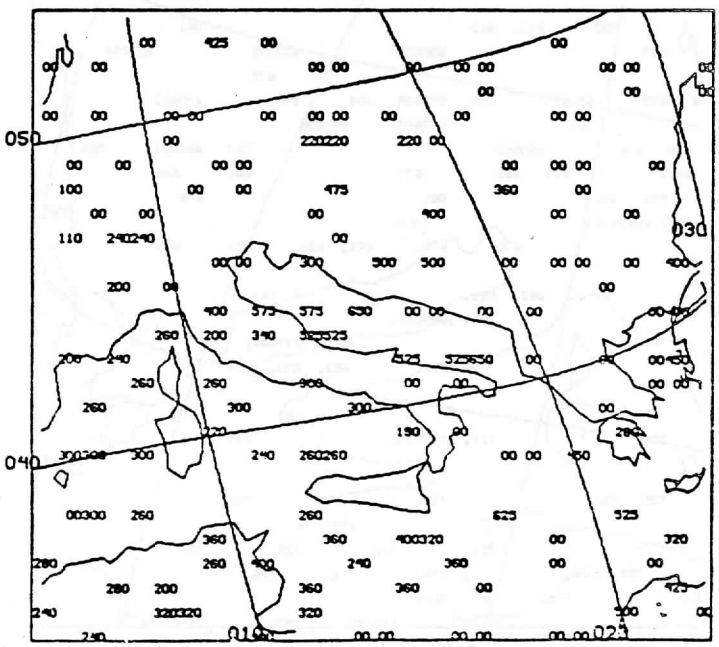

Figure 3d. Cloud top pressure (mb) obtained from GLAS regional scale retrievals.

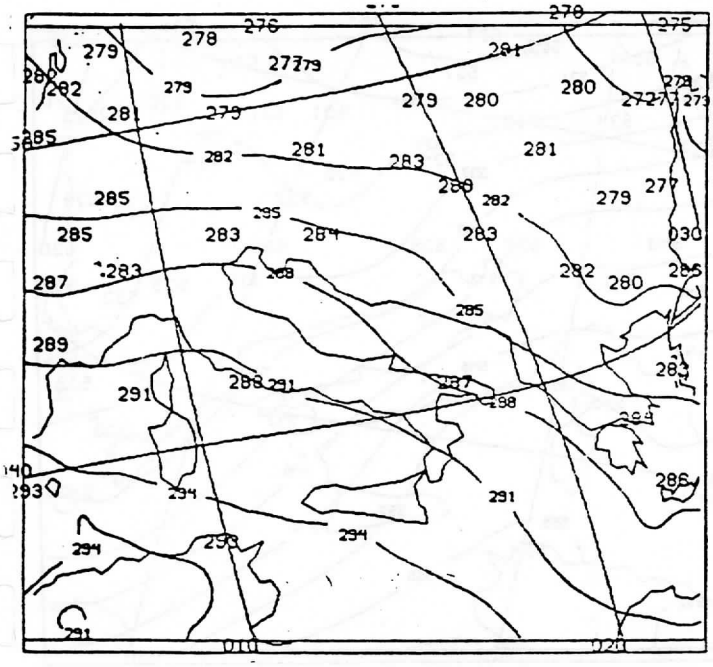

Figure 4a. Contours of 700-1000 mb thickness (decameters) derived from GLAS global scale retrievals. Radiosonde reports are indicated.

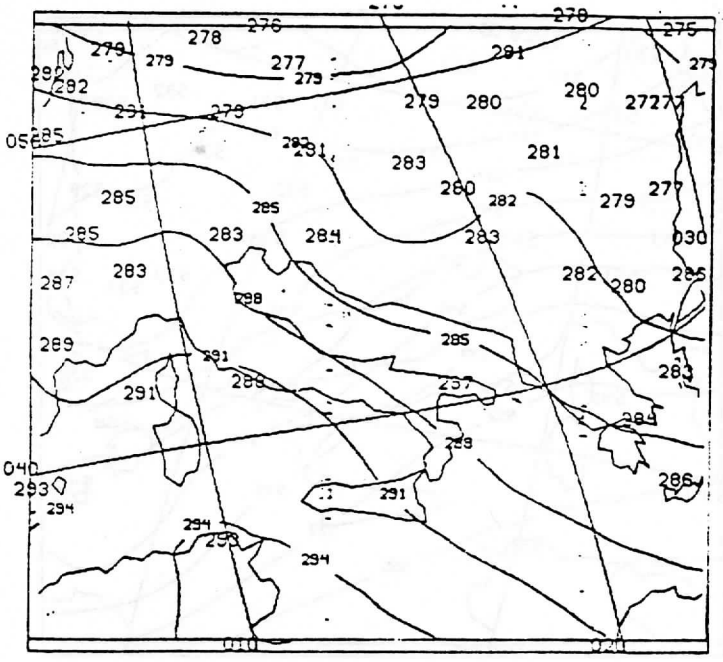

Figure 4b. Same as 4a but for NESDIS operational retrievals.

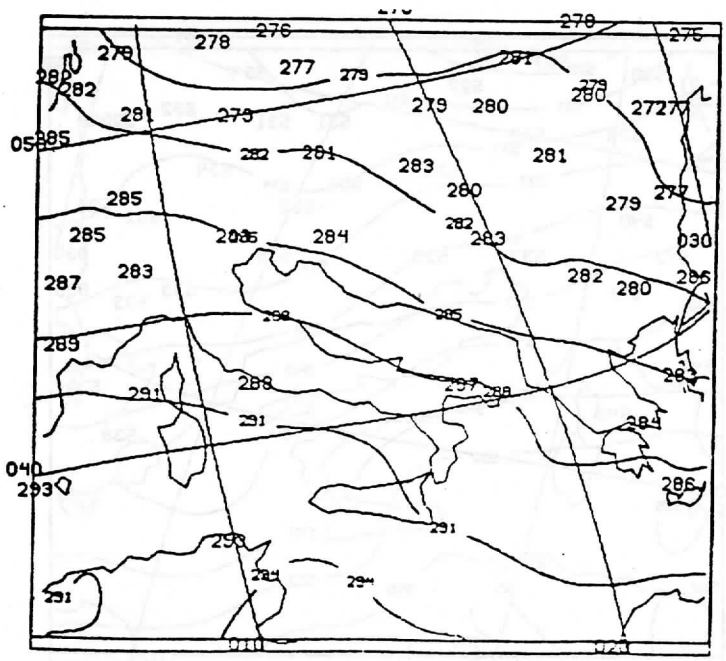

Figure 4c. Same as 4a but for GLAS regional scale retrievals.

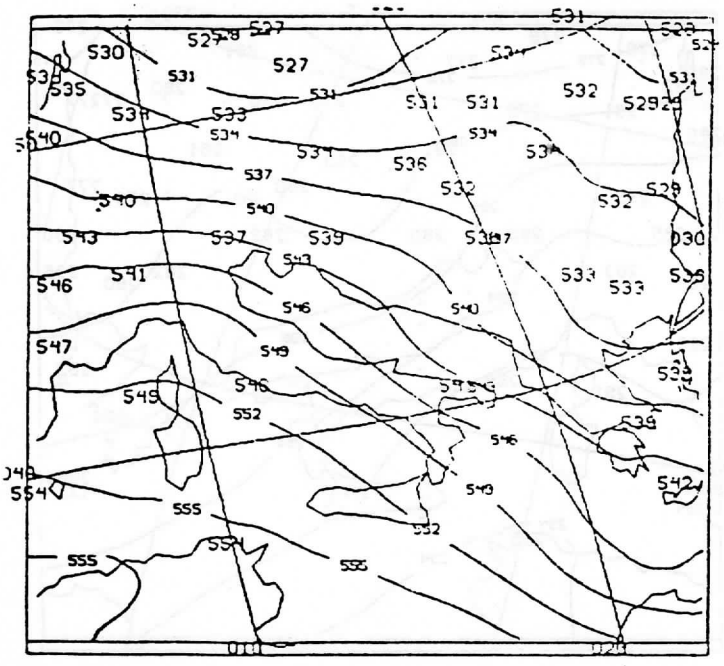

Figure 5a. Contours of 500-100 mb thickness (decameters) from GLAS global scale retrievals. Radiosonde reports are indicated.

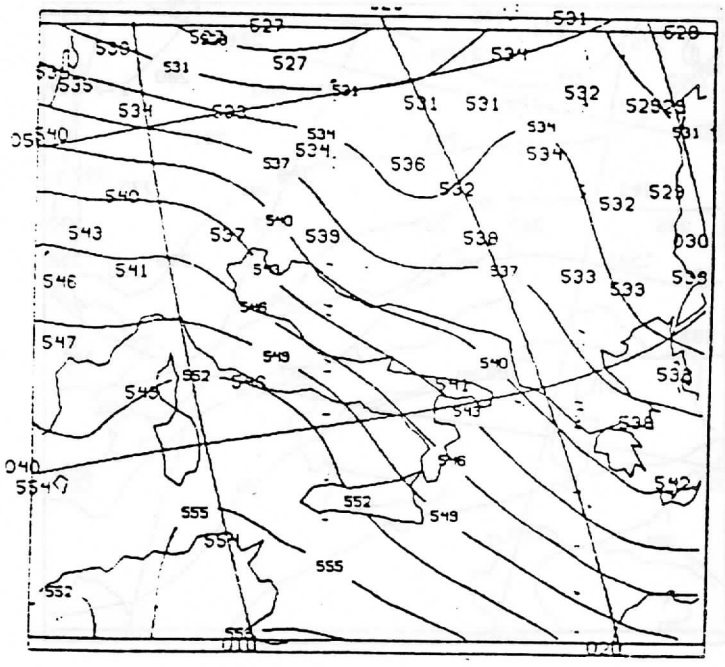

Figure 5b. Same as 5a but for NESDIS operational retrievals.

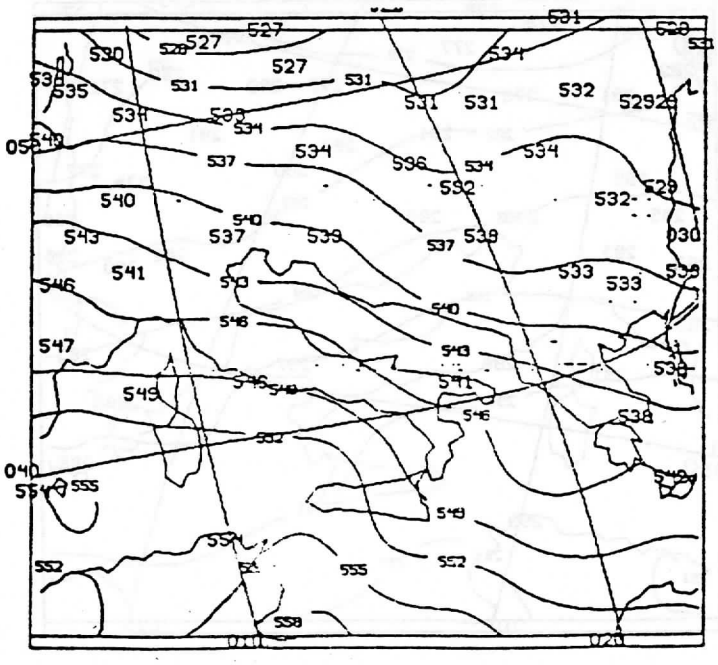

Figure 5c. Same as 5a but for GLAS regional scale retrievals.

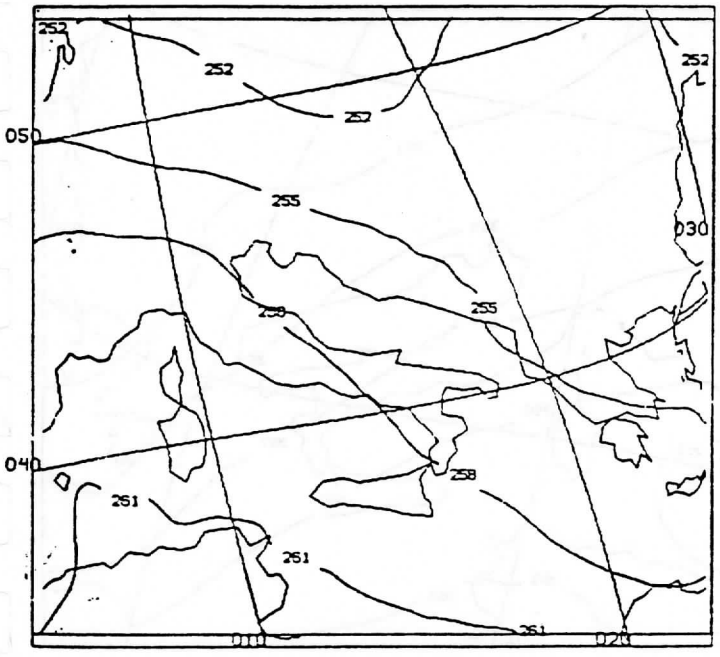

Figure 6a. 700-500 mb thickness contours (decameters) from GLAS global scale retrievals.

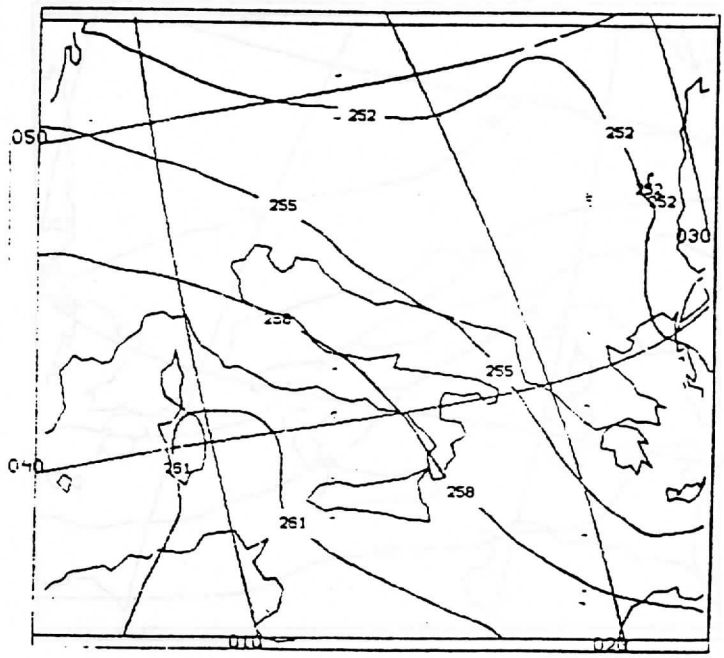

Figure 6b. Same as 6b but for NESDIS operational retrievals.

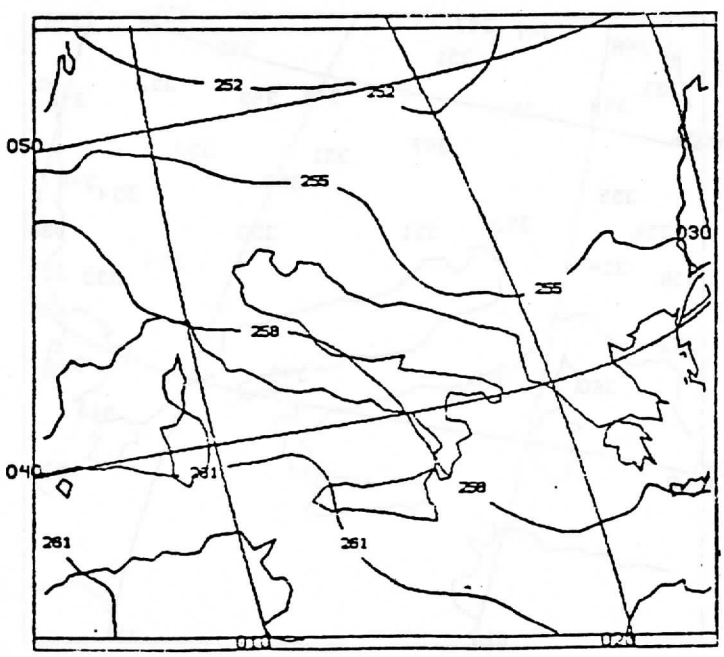

Figure 6c. Same as 6a but for GLAS regional scale retrievals.

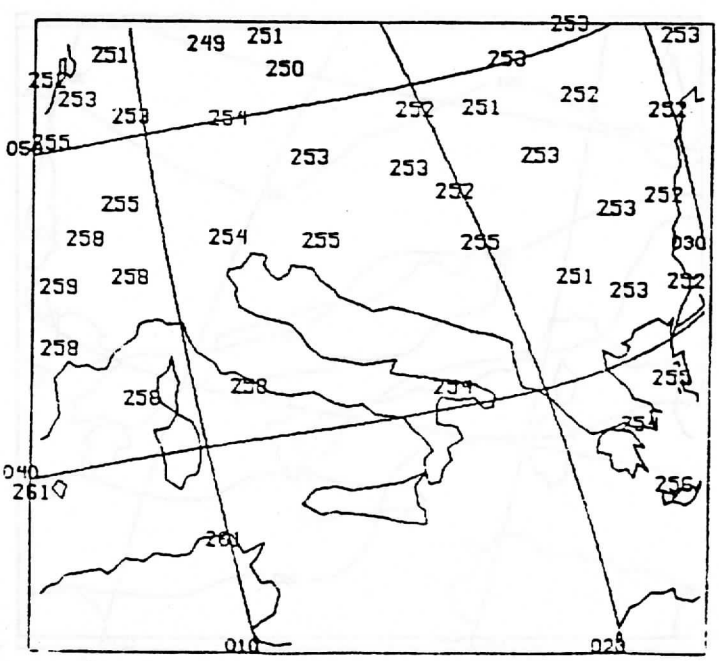

Figure 6d. Colocated radiosonde 700-500 mb thickness reports.

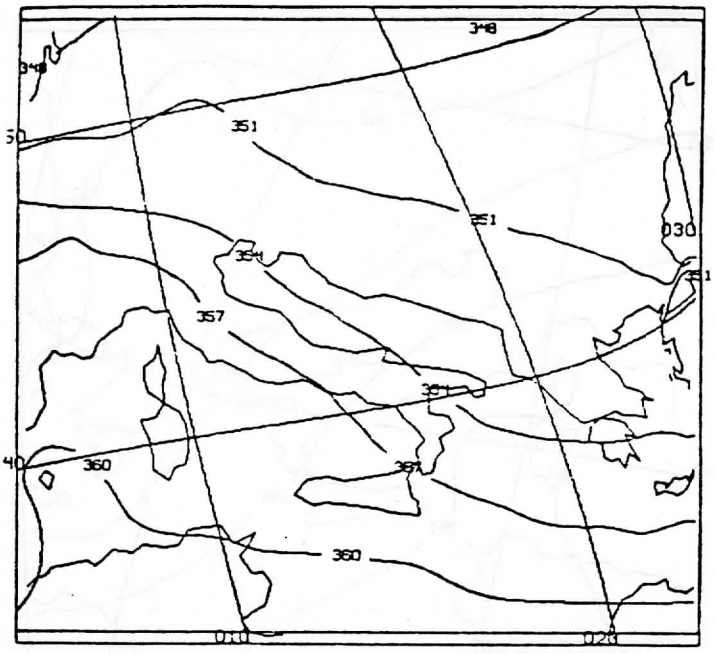

Figure 7a. 500-300 mb thickness contours (decameters) from GLAS global scale retrievals.

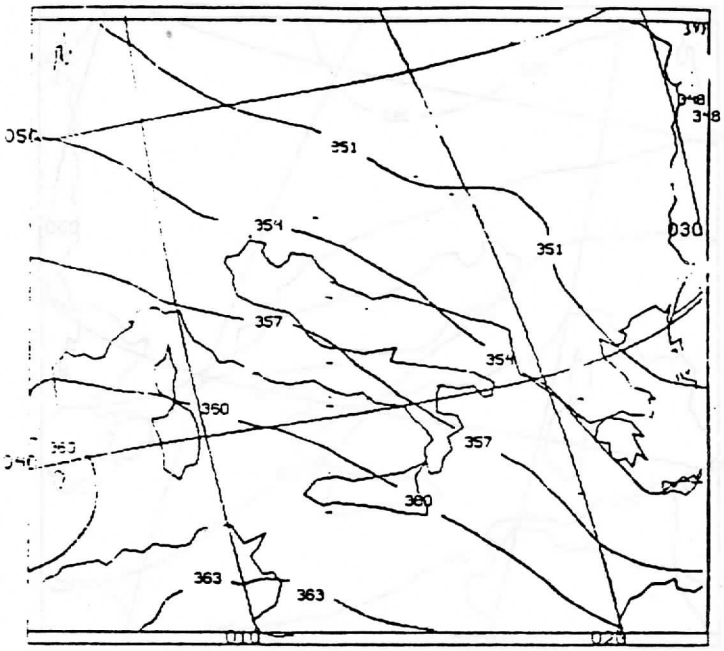

Figure 7b. Same as 7a except for NESDIS operational retrievals.

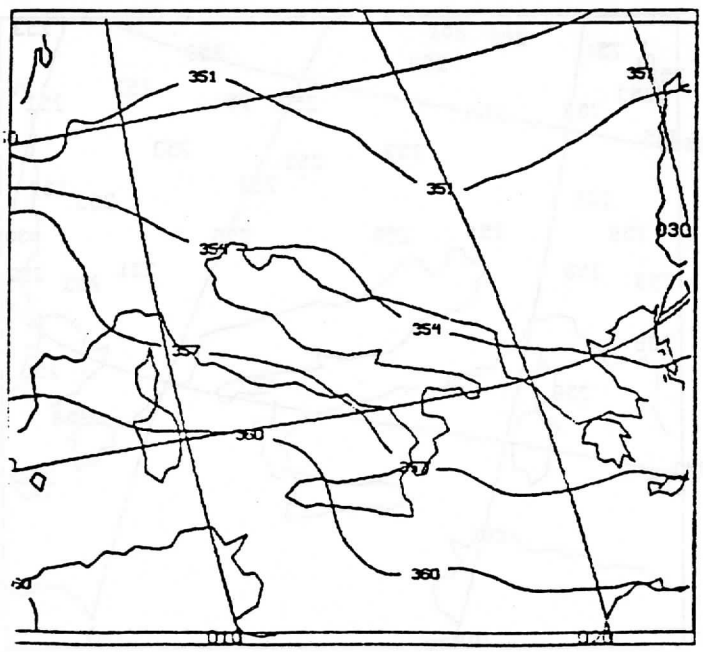

Figure 7c. Same as 7a except for GLAS regional scale retrievals.

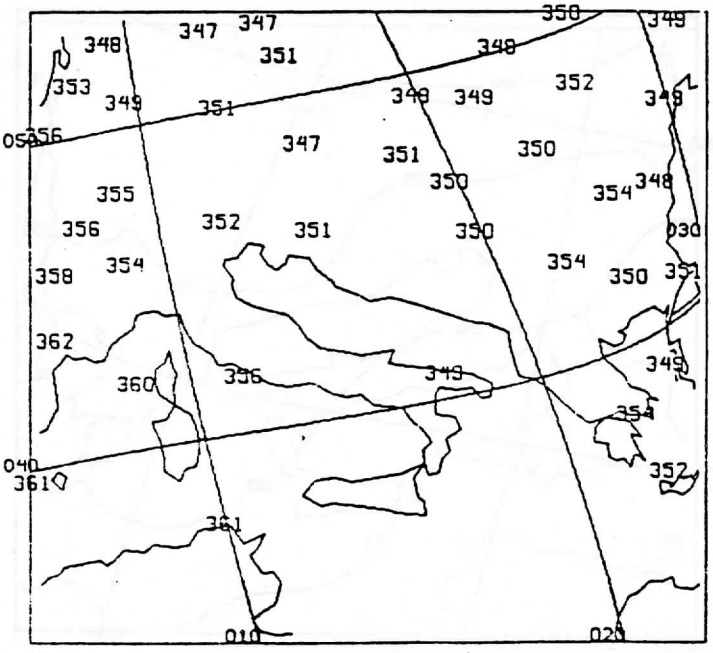

Figure 7d. Colocated radiosonde 500-300 mb thickness reports.

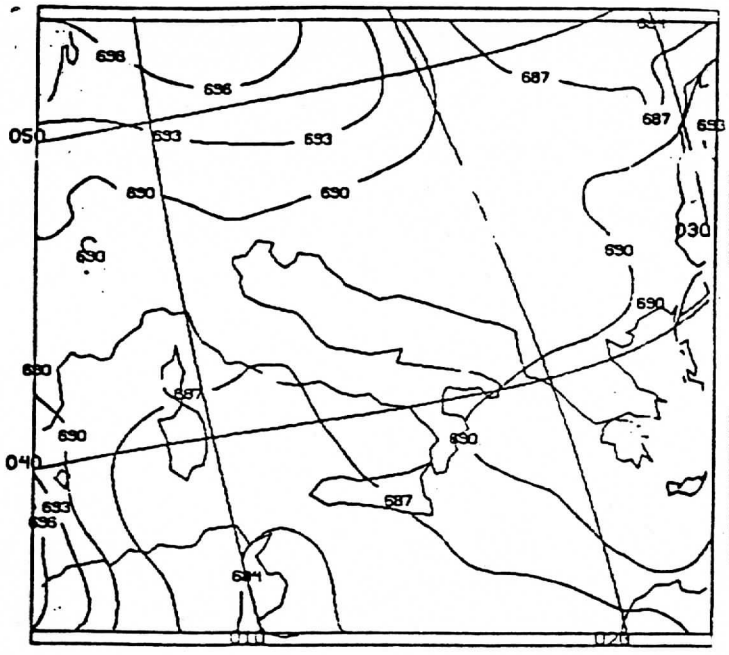

Figure 8a. 300-100 mb thickness contours (decameters) from GLAS global scale retrievals.

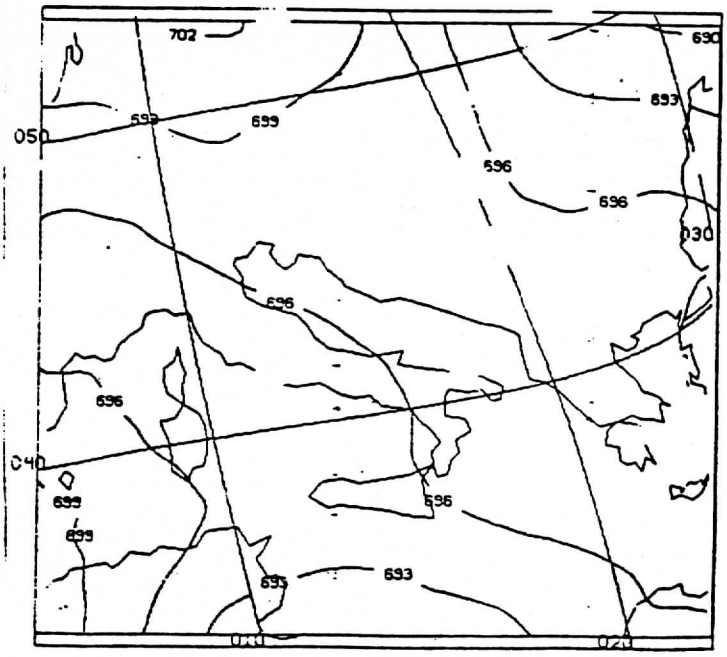

Figure 8b. Same as 8a but for NESDIS operational retrievals.

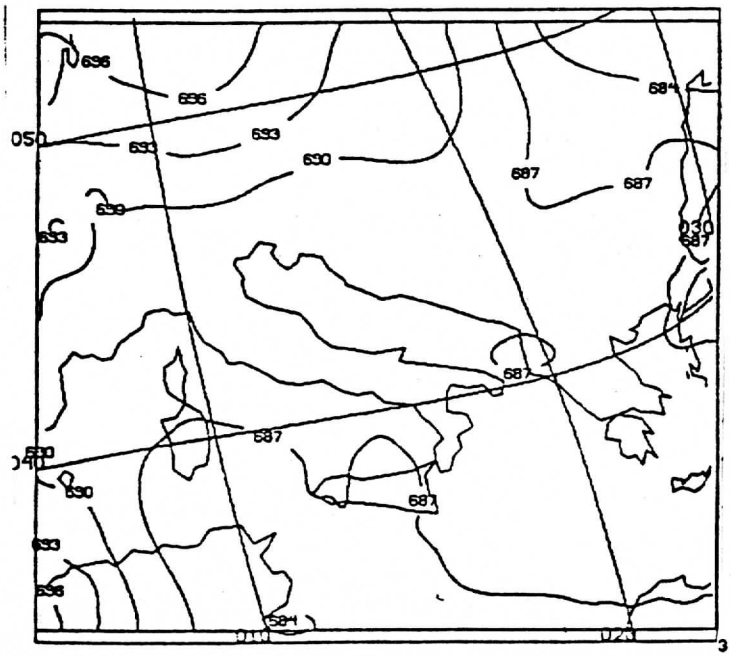

Figure 8c. Same as 8a except for GLAS regional scale retrievals.

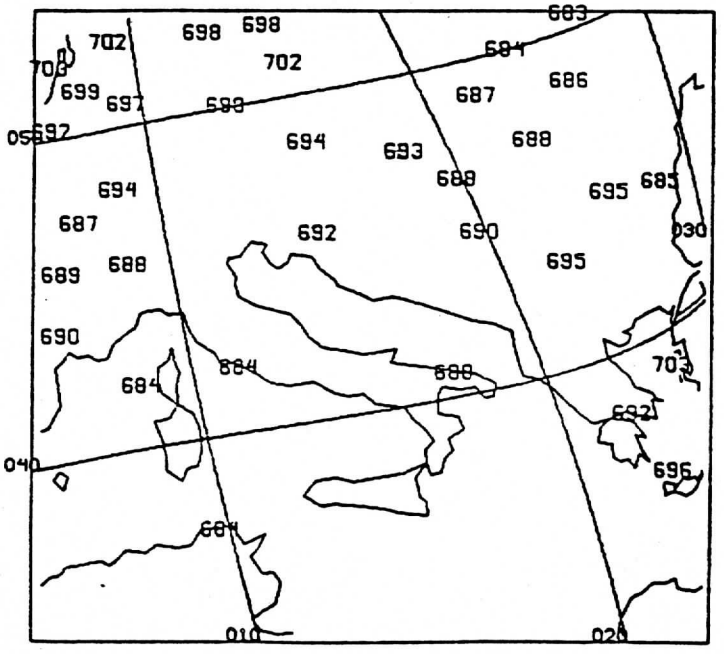

Figure 8d. Colocated radiosonde 300-800 mb thickness reports.

The Technical Proceedings of

The First International TOVS Study Conference

Igls, Austria

29 August through 2 September 1983

Edited by

W. P. Menzel

Cooperative Institute for Meteorological Satellite Studies
Space Science and Engineering Center
University of Wisconsin
1225 West Dayton Street
Madison, Wisconsin 53706
(608)262-0544

March 1984